J|A|C|S
ARTICLES
Published on Web 10/06/2004

Roles of Anionic and Cationic Template Components in Biomineralization of CdS Nanorods Using Self-Assembled DNA−Membrane Complexes

Hongjun Liang, Thomas E. Angelini, Paul V. Braun, and Gerard C. L. Wong*

Contribution from the Department of Materials Science and Engineering, Frederick Seitz Materials Research Laboratory, Department of Physics, University of Illinois at Urbana-Champaign, Urbana, Illinois 61801

Received June 4, 2004; E-mail: gclwong@uiuc.edu

Abstract: Complexes of anionic DNA and cationic liposomes self-assemble into a multilamellar structure where two-dimensional lipid sheets confine a periodic one-dimensional lattice of parallel DNA chains, between which Cd^{2+} ions can condense, and be subsequently reacted with H_2S to form CdS nanorods. In this work, we identify the synergistic roles of the anionic and cationic components within the DNA−membrane template; DNA is highly anionic and condenses the Cd^{2+} ions, while the cationic membrane modulates the concentration of condensed Cd^{2+} ions to control the final CdS nanorod dimensions. Due to the strong electrostatic interactions between the DNA sugar−phosphate backbone and the Cd^{2+} ions, crystallographic control of CdS nanostructures is possible using these simple DNA−membrane templates, which we demonstrate using nanobeam electron diffraction experiments on individual templated CdS nanorods.

1. Introduction

Inorganic materials can be artificially structured at different length scales using biomineralization[1,2] and templating[3−5] techniques. Examples include pioneering work on the use of liquid crystals or surfactants to template mesoporous silica,[6−11] semiconductors,[12−14] and metals,[15,16] templating using bacterial S-layers,[17−21] assembly of inorganics using peptide-based recognition,[22,23] artificial mineralization using synthetic block copolypeptides,[24] block copolymer lithography,[25,26] mineralization of amphiphilic peptides,[27] and biologically inspired micropatterned frameworks.[28] One of the fundamental goals of this field of research is the technology to imitate the exquisite control over morphology and crystalline orientation possible in natural biomineralization. Impressive progress has been made in understanding the role of various polyanionic proteins used in such natural processes.[29−31] However, the identification and isolation of these controlling peptides is difficult, and they are likely to be used together in synergistic combinations in many biomineralization processes. It is therefore interesting to study a simplified prototypical system, by examining the mineralization behavior of biomolecular templates with structures, charge

(1) Addadi, L.; Weiner, S. *Angew. Chem., Int. Ed. Engl.* **1992**, *31*, 153−169.
(2) Mann, S. *Biomineralization: Principles and Concepts in Bioinorganic Materials Chemistry*; Oxford University Press: Oxford, 2002.
(3) Antonietti, M. *Curr. Opin. Colloid Interface Sci.* **2001**, *6*, 244−248.
(4) Brinker, C. J. *Curr. Opin. Colloid Interface Sci.* **1998**, *3*, 166−173.
(5) Soten, I.; Ozin, G. A. *Curr. Opin. Colloid Interface Sci.* **1999**, *4*, 325−337.
(6) Attard, G. S.; Edgar, M.; Goltner, C. G. *Acta Mater.* **1998**, *46*, 751−758.
(7) Kresge, C. T.; Leonowicz, M. E.; Roth, W. J.; Vartuli, J. C.; Beck, J. S. *Nature* **1992**, *359*, 710−712.
(8) Beck, J. S.; Vartuli, J. C.; Kennedy, G. J.; Kresge, C. T.; Roth, W. J.; Schramm, S. E. *Chem. Mater.* **1994**, *6*, 1816−1821.
(9) Monnier, A.; Schuth, F.; Huo, Q.; Kumar, D.; Margolese, D.; Maxwell, R. S.; Stucky, G. D.; Krishnamurty, M.; Petroff, P.; Firouzi, A.; Janicke, M.; Chmelka, B. F. *Science* **1993**, *261*, 1299−1303.
(10) Huo, Q.; Margolese, D. I.; Ciesla, U.; Feng, P.; Gier, T. E.; Sieger, P.; Leon, R.; Petroff, P. M.; Schuth, F.; Stucky, G. D. *Nature* **1994**, *368*, 317−321.
(11) Firouzi, A.; Kumar, D.; Bull, L. M.; Besier, T.; Sieger, P.; Huo, Q.; Walker, S. A.; Zasadzinski, J. A.; Glinka, C.; Nicol, J.; Margolese, D.; Stucky, G. D.; Chmelka, B. F. *Science* **1995**, *267*, 1138−1143.
(12) Braun, P. V.; Osenar, P.; Stupp, S. I. *Nature* **1996**, *380*, 325−328.
(13) Stupp, S. I.; Braun, P. V. *Science* **1997**, *277*, 1242−1248.
(14) Murray, C. B.; Kagan, C. R.; Bawendi, M. G. *Science* **1995**, *270*, 1335−1338.
(15) Attard, G. S.; Bartlett, P. N.; Coleman, N. R. B.; Elliott, J. M.; Owen, J. R.; Wang, J. H. *Science* **1997**, *278*, 838−840.
(16) Attard, G. S.; Goltner, C. G.; Corker, J. M.; Henke, S.; Templer, R. H. *Angew. Chem., Int. Ed. Engl.* **1997**, *36*, 1315−1317.
(17) Douglas, K.; Clark, N. A.; Rothschild, K. J. *Appl. Phys. Lett.* **1986**, *48*, 676−678.
(18) Douglas, K.; Clark, N. A.; Rothschild, K. J. *Appl. Phys. Lett.* **1990**, *56*, 692−694.
(19) Schultze-Lam, S.; Fortin, D.; Davis, B. S.; Beveridge, T. J. *Chem. Geol.* **1996**, *132*, 171−181.
(20) Schultze-Lam, S.; Harauz, G.; Beveridge, T. J. *J. Bacteriol.* **1992**, *174*, 7971−7981.
(21) Shenton, W.; Pum, D.; Sleytr, U. B.; Mann, S. *Nature* **1997**, *389*, 585−587.
(22) Brown, S. *Proc. Natl. Acad. Sci. U.S.A.* **1992**, *89*, 8651−8655.
(23) Whaley, S. R.; English, D. S.; Hu, E. L.; Barbara, P. F.; Belcher, A. M. *Nature* **2000**, *405*, 665−668.
(24) Cha, J. N.; Stucky, G. D.; Morse, D. E.; Deming, T. J. *Nature* **2000**, *403*, 289−292.
(25) Park, M.; Harrison, C.; Chaikin, P. M.; Register, R. A.; Adamson, D. H. *Science* **1997**, *276*, 1401−1404.
(26) Thurn-Albrecht, T.; Schotter, J.; Kastle, C. A.; Emley, N.; Shibauchi, T.; Krusin-Elbaum, L.; Guarini, K.; Black, C. T.; Tuominen, M. T.; Russell, T. P. *Science* **2000**, *290*, 2126−2129.
(27) Hartgerink, J. D.; Samuel, E. B.; Stupp, I. *Science* **2001**, *294*, 1684−1688.
(28) Aizenberg, J.; Muller, D. A.; Grazul, J. L.; Hamann, D. R. *Science* **2003**, *299*, 1205−1208.
(29) Belcher, A. M.; Wu, X. H.; Christensen, R. J.; Hansma, P. K.; Stucky, G. D.; Morse, D. E. *Nature* **1996**, *381*, 56−58.
(30) Shimizu, K.; Cha, J.; Stucky, G. D.; Morse, D. E. *Proc. Natl. Acad. Sci. U.S.A.* **1998**, *95*, 6234−6238.
(31) Cha, J. N.; Shimizu, K.; Zhou, Y.; Christiansen, S. C.; Chmelka, B. F.; Stucky, G. D.; Morse, D. E. *Proc. Natl. Acad. Sci. U.S.A.* **1999**, *96*, 361−365.

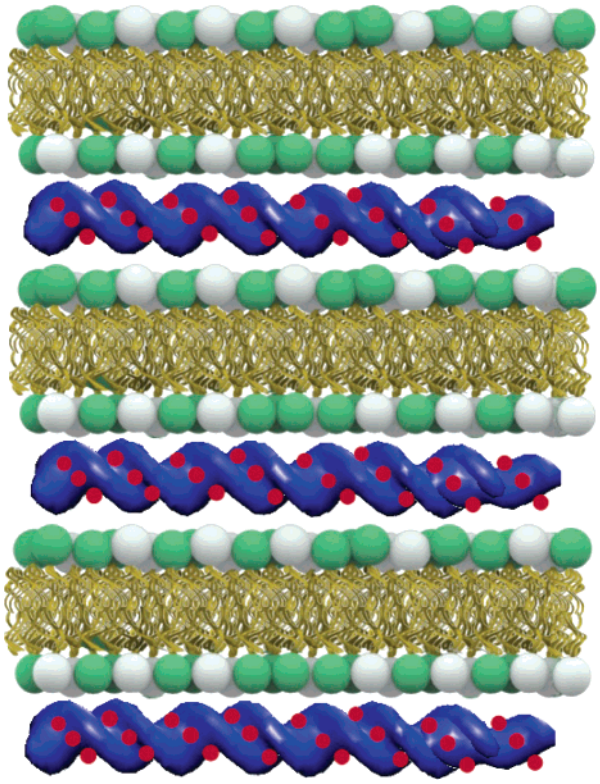

Figure 1. Schematic representation of CdS growth within DNA−membrane complexes: the Cd^{2+} ions (red balls) are organized by DNA strands (blue) in the lamellar DNA−membrane complexes (side-view) and subsequently react with H_2S (not shown) to form CdS nanorods that have tiled (002) polar planes parallel to the negatively charged sugar−phosphate backbone of DNA.

distributions, phase behavior, and self-assembly characteristics that can be controlled precisely.

In this paper, we systematically investigate semiconducting CdS nanorod growth within self-assembled DNA-membrane templates, in which Cd^{2+} ions are organized and subsequently reacted with H_2S to form CdS nanorods,[32] as shown in Figure 1. Specifically, we examine the interplay between the anionic and cationic components of the template and how the templated CdS nanorods are affected when the charge of the membrane is tuned relative to the charge of the DNA, as well as when the degree of overcharging is varied for both positively and negatively charged templates. To find out how geometrically tolerant the templating process is, the influence of DNA polydispersity on the template structure has also been assessed. The number of Cd^{2+} precursor ions condensed within the templates for different conditions has been directly measured and correlated with the DNA−membrane template structure, as well as the resultant nanorod morphology, which has been monitored using synchrotron X-ray diffraction and transmission electron microscopy. Depending on the charge of the membrane, different concentrations of Cd^{2+} ions are condensed into the template, and different morphologies of CdS are templated. The condensed Cd^{2+} ion concentration is also controlled by the degree of template overcharging away from the DNA−cationic membrane isoelectric point. Interestingly, no significant amount of Cd^{2+} is condensed for positively overcharged templates, despite the existence of highly anionic DNA and short screening Debye lengths. In contrast, for isoelectric and negatively overcharged templates, the condensed Cd^{2+} ion concentrations are high inside the nanopores defined by adjacent DNA strands confined between cationic membrane sheets and can be as much as 2.5 M, which is almost 100× greater than that of the ambient concentrations. Finally, we show that crystallographic control of inorganic nanostructures is possible using these simple DNA−membrane templates by performing nanobeam electron diffraction experiments on individual templated CdS nanorods.

Self-assembled complexes comprised of anionic polyelectrolytes and cationic lipids have recently received intense experimental and theoretical attention.[33−48] DNA−membrane complexes were originally conceived as nonviral gene delivery systems.[49,50] The addition of DNA to cationic liposomes induces a topological transition from liposomes to condensed, birefringent liquid crystalline globules with a novel multilamellar structure, in which a periodic one-dimensional (1D) lattice of parallel DNA chains is confined between stacked two-dimensional (2D) lipid sheets.[36] Lamellar (L^C_α) DNA−membrane complexes constitute a new hybrid state of matter, where a 2D smectic liquid crystalline phase is coupled to a 3D smectic liquid crystalline phase. Other types of lamellar polyelectrolyte-membrane structures have been reported, such as the unexpected "missing layer" super-lattice structure of actin−membrane complexes,[39] which consist of a swollen periodic stack of composite three-layer polyelectrolyte-membrane sheets in which each membrane bilayer is associated with two layers of actin, one on each hydrophilic surface. Moreover, by lowering the membrane's bending rigidity or by changing its spontaneous curvature, an inverted hexagonal phase with a dramatically enhanced tendency for membrane fusion can be formed, in which DNA chains coated by lipid monolayers are packed into a 2D columnar hexagonal array.[46] During condensation of these complexes, the cationic lipid headgroups neutralize the phosphate groups on the DNA chains, effectively replacing the originally Manning condensed counterions and, consequently, driving this higher order self-assembly.

These DNA−membrane complexes constitute a new class of tunable nanostructured materials with intriguing technological possibilities, in addition to their inherent fundamental interest for gene therapy and soft condensed matter physics. The interhelical distance between DNA chains in the 1D lattice

(32) Liang, H.; Angelini, T. E.; Ho, J.; Braun, P. V.; Wong, G. C. L. *J. Am. Chem. Soc.* **2003**, *125*, 11786−11787.

(33) Dan, N. *Biochim. Biophys. Acta-Biomembranes* **1998**, *1369*, 34−38.
(34) Bruinsma, R.; Mashl, J. *Europhys. Lett.* **1998**, *41*, 165−170.
(35) Subramanian, G.; Hjelm, R. P.; Deming, T. J.; Smith, G. S.; Li, Y.; Safinya, C. R. *J. Am. Chem. Soc.* **2000**, *122*, 26−34.
(36) Radler, J. O.; Koltover, I.; Salditt, T.; Safinya, C. R. *Science* **1997**, *275*, 810−814.
(37) Ponomarenko, E. A.; Waddon, A. J.; Bakeev, K. N.; Tirrell, D. A.; MacKnight, W. J. *Macromolecules* **1996**, *29*, 4340−4345.
(38) Antonietti, M.; Conrad, J.; Thuenemann, A. *Macromolecules* **1994**, *27*, 6007−6011.
(39) Wong, G. C. L.; Tang, J. X.; Lin, A.; Li, Y.; Janmey, P. A.; Safinya, C. R. *Science* **2000**, *288*, 2035−2039.
(40) Koltover, I.; Salditt, T.; Safinya, C. R. *Biophys. J.* **1999**, *77*, 915−924.
(41) Lasic, D. D.; Strey, H.; Stuart, M. C. A.; Podgornik, R.; Frederik, P. M. *J. Am. Chem. Soc.* **1997**, *119*, 832−833.
(42) May, S.; Ben-Shaul, A. *Biophys. J.* **1997**, *73*, 2427−2440.
(43) Bruinsma, R. *Eur. Phys. J. B* **1998**, *4*, 75−88.
(44) Harries, D.; May, S.; Gelbart, W. M.; Ben-Shaul, A. *Biophys. J.* **1998**, *75*, 159−173.
(45) Koltover, I.; Wagner, K.; Safinya, C. R. *Proc. Natl. Acad. Sci. U.S.A.* **2000**, *97*, 14046−14051.
(46) Koltover, I.; Salditt, T.; Radler, J. O.; Safinya, C. R. *Science* **1998**, *281*, 78−81.
(47) Golubovic, L.; Golubovic, M. *Phys. Rev. Lett.* **1998**, *80*, 4341−4344.
(48) O'Hern, C. S.; Lubensky, T. C. *Phys. Rev. Lett.* **1998**, *80*, 4345−4348.
(49) Felgner, P. L. *Sci. Am.* **1997**, *276*, 102−106.
(50) Friedmann, T. *Sci. Am.* **1997**, *276*, 96−101.

intercalated between the lamellar membrane sheets can be tuned between 2.5 and 6.0 nm by changing the relative proportion of cationic and neutral lipids. DNA within these lamellar complexes can condense in the presence of divalent counterions into close-packed rafts.[45] In this work, we use Cd^{2+}, the cationic component of CdS, to drive this 2D DNA condensation within the membrane lipid galleries. Since the Cd^{2+} ions are confined and organized by the inter-DNA nanopores, we can use the DNA−membrane complex as a nanoreactor to template the growth of CdS nanorods via reaction with H_2S.

2. Materials and Methods

2.1. DNA Preparation. Two kinds of DNA were used. Monodispersed λ-phage DNA (500 μg/mL in 10mM Tris-HCl, 1mM EDTA, PH=8 buffer, from New England Biolabs, Inc., Beverly, MA. Mw=3.15×10^7 daltons, 48,502 base pairs) was precipitated out using standard procedure[51] and dissolved in Millipore water at 10 mg/mL. Poly-dispersed Calf Thymus DNA (solid fibrous form, from Amersham Biosciences, Piscataway, NJ., average MW = 5×10^7 daltons, 75 000 base pairs) was first dissolved in pH = 8 TE buffer, then precipitated out using the same protocol as mentioned above to further purify. The purified Calf Thymus DNA was dissolved in Millipore water at 10 mg/mL. Freshly prepared DNA solution was stored at 4 °C and used within one week. The DNA concentration was determined by UV−vis.[52]

2.2. Liposome Preparation. The positively charged lipid dioleoyl trimethylammonium propane (DOTAP) and the neutral lipid dioleoyl phosphatidyl choline (DOPC) with the same alkyl chain length were used (both from Avanti Polar Lipids, Alabaster, AL). Membrane charge density was controlled by the DOTAP/DOPC ratio. To prepare liposomes with a given surface charge density, stock solutions of DOTAP at 30 mg/mL (dissolved in 90/10 chloroform/methanol) were first mixed with stock solutions of DOPC at 30 mg/mL (dissolved in chloroform) at the desired ratio. The mixture was dried in N_2 and then desiccated under vacuum overnight. Millipore water (18.2 MΩ) was added to the dried lipids to obtain liposome solutions with final concentrations of 40 mg/mL. The liposome solution was then incubated at 37 °C overnight and then sonicated to clarity (ultrasonic processor from Sonics & Materials, Inc., Newtown, CT). The resultant solution was extruded through a 0.2 μm pore size Nucleopore filter. Freshly prepared liposome solutions were stored at 4 °C and used within 1 week.

2.3. DNA−Membrane Complexes Preparation. DNA, lipid, and $CdCl_2$ stock solutions were added together into a microcentrifuge tube and mixed to form DNA membrane complexes at different charge stoichiometries and different global Cd^{2+} concentrations. The DNA to lipid charge stoichiometry (D/L ratio) is defined as the total negative charge of the phosphate groups on DNA divided by the total positive charge of the cationic DOTAP headgroups in the membrane. The DNA−membrane complexes are defined as isoelectric when $D/L = 1$, as negatively overcharged when $D/L > 1$, and as positively overcharged when $D/L < 1$.

2.4. X-ray Diffraction (XRD). All DNA−membrane complexes were sealed in a 1.5 mm quartz capillary for XRD. Wide-angle X-ray scattering (WAXS) was measured using a Bruker general area detector diffraction system equipped with a four-circle diffractometer and Hi-Star multiwire area detector. Small-angle X-ray scattering (SAXS) was measured using our in-house spectrometer as well as at Beamline 4-2 at Stanford Synchrotron Radiation Laboratory (SSRL). For the in-house experiments, incident Cu Kα radiation (λ = 1.54 Å) from a Rigaku rotating-anode generator is monochromatized and focused using Osmic confocal multilayer optics (Confocal Max-Flux) and defined using four sets of slits so that the final beam size at the sample position is approximately 0.8×0.8 mm^2. Scattered radiation is collected on a Bruker Hi-Star 2-D multiwire detector (pixel size 105 μm). All flight paths except for the sample position are in a vacuum to reduce air scattering. For the SSRL experiments, incident synchrotron X-rays from the BL-4-2 8-pole Wiggler have been monochromatized using a double-bounce Si(111) crystal (λ = 1.3806 Å) and focused using a cylindrical mirror, and the scattered radiation is collected using an MAR Research CCD camera (pixel size 79 μm). The 2D SAXS data from both setups are mutually consistent.

2.5. Inductively Coupled Plasma Optical Emission Spectroscopy (ICPOES). Since DNA−membrane complexes precipitate out of solution, the Cd^{2+} concentration within the complexes can be inferred by measuring the characteristic Cd emission intensity of the supernatant using ICPOES. The spectrometer was calibrated using $CdCl_2$ solutions of known concentrations (0 to 20 ppm). For each complex at known global [Cd^{2+}], the complex was precipitated by ~1200 g centrifugation. The supernatant was collected and filtered by YM-10 Centricon filters (Millipore). To minimize errors from residual salts in the filter, the filters for each individual measurement were rinsed with Millipore water after use, and the rinsing solution was collected and used to dilute the supernatant until the concentration [Cd^{2+}] of diluted supernatant fell into the calibrated range of ICPOES. A control sample was also made at exactly the same manner as the complex, only without the DNA−membrane complex. The [Cd^{2+}] for each pair (diluted supernatant of sample and control) was measured by ICPOES and compared against the calibrated curve. The number of Cd^{2+} ions inside the complex at each global [Cd^{2+}] was calculated by comparing the different measured [Cd^{2+}] for each pair. The Cd^{2+} ions density inside DNA−membrane complexes was represented as number of Cd^{2+} ions per base pair of DNA (#Cd^{2+}/bp).

2.6. Templated Growth of CdS Nanocrystals. DNA-membrane complexes with different [Cd^{2+}] were reacted with H_2S gas (C. P. 99.5%) at ambient temperature and pressure. H_2S flow was controlled by a needle valve and humidified by passing through a gas washing bottle before purging the complexes. The gas flow rate was monitored via a gas bubbling tube. The reaction $Cd^{2+} + H_2S \rightarrow CdS + 2H^+$ converted Cd^{2+} ionic precursors in the complexes into CdS. After the reaction, the complexes were rinsed with Millipore water to wash away the CdS grown outside the DNA−membrane complexes (for example, in the free solution or on surface of the complexes). The DNA−membrane complexes with CdS grown inside were dissolved in a 1% sodium dodecyl sulfate (SDS) solution and centrifuged to collect the CdS nanocrystals. The centrifuged pellet was washed and centrifuged iteratively to further remove remaining organics.

2.7. Transmission Electron Microscope (TEM). The CdS nanocrystals were dispersed in Millipore water with the aid of sonication. A droplet of the CdS-dispersed solution was put on a 200 mesh size holy carbon grid (from SPI, West Chester, PA) and dried on filter paper. The samples were investigated using a JEOL 2010F energy filtering, field-emission analytic TEM/STEM operating at 200 kV. The TEM is controlled by the JEOL FasTEM system. Images were taken using a CCD camera on a Gatan image filter (GIF), and diffraction patterns were collected using a Fuji image plate (pixel size 25 μm).

3. Results and Discussions

3.1. Isoelectric Complexes with and without Cd^{2+} Ions. We start with a detailed characterization of the initial state before reaction, the DNA−membrane template structure with condensed Cd^{2+} ions before they are reacted to form CdS. These parent complexes assembled from DOTAP/DOPC lipids are lamellar, and the 1D DNA lattice spacing (d_{DNA}) within the lipid galleries is controlled by the membrane charge density, determined by the DOTAP/DOPC ratio.[36] The structures of isoelectric

(51) Sambrook, J.; Fritsch, E. F.; Maniatis, T. *Molecular Cloning, A Laboratory Manual*, 2nd ed.; Cold Spring Harbor Laboratory Press: 1989.
(52) Switzer, R. L.; Garrity, L. F. *Exerimental Biochemistry*, 3rd ed.; W. H. Freeman and Company: New York, 2003.

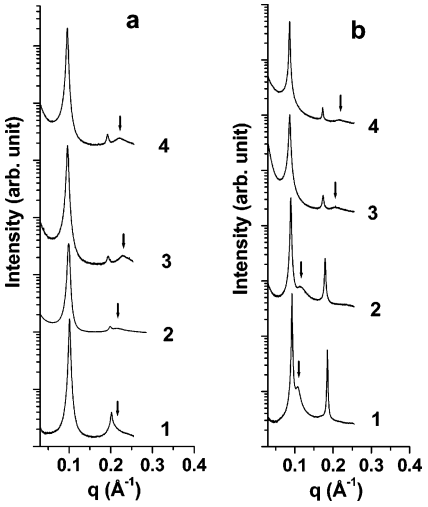

Figure 2. SAXS data for isoelectric λ-phage DNA−membrane complexes at different membrane charge densities and global [Cd^{2+}]: (a) 70/30 DOTAP/DOPC; (b) 30/70 DOTAP/DOPC. Curves 1, 2, 3, and 4 on each of the data sets correspond to global [Cd^{2+}] at 0, 10, 30, and 40 mM, respectively. The sharp, regularly spaced peaks correspond to the lamellar organization. The arrows indicate the positions of the in-plane inter-DNA correlation peaks. Note the large change in the DNA peak positions for the lower membrane charge density complex (b), due to the condensation of DNA into close-packed 2D rafts.

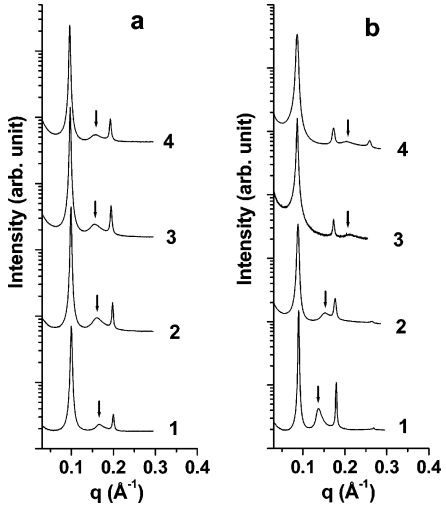

Figure 3. SAXS for overcharged λ-phage DNA−membrane complexes at different membrane charge densities and global [Cd^{2+}]. (a) Positively overcharged 70/30 DOTAP/DOPC complexes, $D/L = 0.6$; (b) negatively overcharged 30/70 DOTAP/DOPC complexes, $D/L = 1.4$. Curves 1, 2, 3, and 4 for both data sets correspond to global [Cd^{2+}] at 0, 10, 30, and 40 mM, respectively. The arrows indicate the positions of the in-plane inter-DNA correlation peaks. Note the large change in the DNA peak positions in the negatively overcharged complexes (b), due to the condensation of DNA into close-packed 2D rafts within the lipid galleries. Note also the absence of the DNA condensation transition for the positively overcharged complex (a).

λ-phage DNA−membrane complexes at different global [Cd^{2+}] were studied by SAXS. We observe the 2D collapse of DNA into close-packed condensed rafts within isoelectric complexes at high global [Cd^{2+}] for all the membrane charge densities studied.

Two typical sets of SAXS data at different membrane charge densities and global [Cd^{2+}] are shown in Figure 2. The two regularly spaced sharp peaks correspond to the 1st and 2nd order of the lamellar correlation. For DNA-membrane complexes comprised of 70/30 DOTAP/DOPC membranes without added Cd^{2+} (see curve 1 in Figure 2 a), the peaks correspond to a lamellar periodicity of 62.2 Å, which corresponds to the membrane bilayer thickness (37.2 Å for 70/30 DOTAP/DOPC) plus the diameter of hydrated DNA (25 Å). For complexes with 30/70 DOTAP/DOPC membranes without added Cd^{2+} (see curve 1 Figure 2 b), the peaks correspond to a lamellar periodicity of 67.8 Å, which is again the membrane bilayer thickness (42.8 Å for 30/70 DOTAP/DOPC) plus the diameter of hydrated DNA (25 Å). The peaks under the arrow correspond to the in-plane DNA correlation. For both membrane charge densities, DNA is observed to condense at elevated global [Cd^{2+}], evidenced by a large change in the inter-DNA distance in the 1D lattice. For the high membrane charge density sample (DOTAP/DOPC = 70/30) with no added Cd^{2+}, the inter-DNA spacing is initially 29.8 Å, which is close to 25 Å, the diameter for hydrated DNA (see curve 1 in Figure 2a). When global [Cd^{2+}] was increased, this peak shifted to higher q. The final condensed d_{DNA} is 28.4 Å at global [Cd^{2+}] = 40 mM (see curve 4 in Figure 2a), which is just enough to fit one diameter of hydrated DNA rod plus one diameter of hydrated Cd^{2+} ions (∼4 Å). For the low membrane charge density complexes (DOTAP/DOPC = 30/70), the initial DNA separation is significantly larger than the DNA diameter (d_{DNA} = 58.1 Å; see curve 1 in Figure 2b). When the global [Cd^{2+}] is increased beyond a threshold value, this DNA spacing decreased sharply. The most drastic decrease occurs near [Cd^{2+}]=30 mM, where d_{DNA} drops to 30.5 Å from an initial value of 58.1 Å. Further increases of the global [Cd^{2+}] to 40 mM only causes a small decrease of the DNA spacing, resulting in a final condensed DNA spacing of 28.8 Å, which is similar to that for complexes with 70/30 DOTAP/DOPC membrane. The lamellar spacing is slightly expanded as global [Cd^{2+}] is increased. The observed expansion of the lamellar spacing after DNA condensation is 2.6 and 4.9 Å for the DOTAP/DOPC = 70/30 and DOTAP/DOPC = 30/70 complexes, respectively. This is likely due to the additional Cd^{2+} ions that were organized into the complex, along with their associated hydration layers. Since typical hydrated diameters of divalent ions (∼4 Å) are significantly smaller than the surface-to-surface distance between membranes in the complex (∼25 Å), this observed expansion of the lamellar spacing suggests that the ions are organized not just in the 2D plane but along the layering direction as well. The degree of expansion along the layering direction after DNA condensation is different for complexes with different membrane charge densities. This suggests that different densities of Cd^{2+} ions can be accommodated in complexes with the same inter-DNA distances. This is in fact consistent with the measurements of condensed Cd^{2+} ion density described below.

3.2. Nonisoelectric Complexes with and without Cd^{2+} Ions. By changing the ratio of DNA charge to lipid charge (by making the complexes positively overcharged or negatively overcharged), the initial DNA separation d_{DNA} can be tuned, while maintaining the basic lamellar structure. Overcharged (nonisoelectric) λ-phage DNA−membrane complexes at different global [Cd^{2+}] have been studied using SAXS. The lamellar phase is preserved, and the characteristic diffraction signature of a regularly spaced series of diffraction peaks can clearly be observed. For positively overcharged complexes (70/30 DOTAP/DOPC membrane charge density) without added Cd^{2+} (see curve 1 in Figure 3a), the peaks correspond to a lamellar periodicity of 62.8 Å; for negatively overcharged complexes

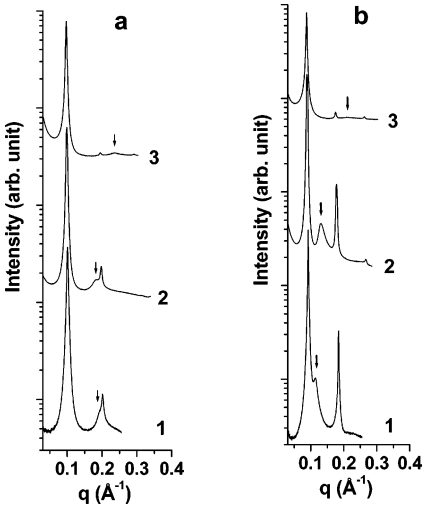

Figure 4. DNA−membrane complexes with polydisperse DNA and DNA−membrane complexes with monodisperse DNA exhibit similar condensation behavior in the presence of Cd^{2+} ions. SAXS data for isoelectric calf thymus DNA−membrane complexes at different membrane charge densities and global [Cd^{2+}]. (a) 70/30 DOTAP/DOPC; (b) 30/70 DOTAP/DOPC. Curves 1, 2, and 3 correspond to global [Cd^{2+}] at 0, 10, and 40 mM, respectively. Peaks under arrows indicate in-plane DNA correlation peaks. Note the large change in the DNA peak positions in the lower membrane charge density complexes (b), due to the condensation of DNA into close-packed 2D rafts, similar to the corresponding behavior with monodisperse λ-DNA.

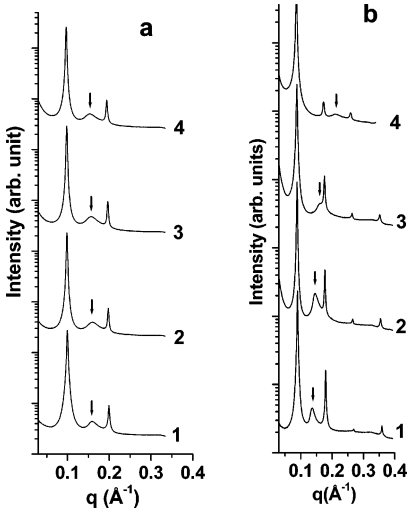

Figure 5. SAXS for overcharged calf thymus DNA−membrane complexes at different membrane charge densities and global [Cd^{2+}]. (a) Positively overcharged 70/30 DOTAP/DOPC complexes, $D/L = 0.6$; (b) Negatively overcharged 30/70 DOTAP/DOPC complexes, $D/L = 1.4$. Curves 1, 2, 3, and 4 for both data sets correspond to global [Cd^{2+}] at 0, 10, 30, and 40 mM, respectively. The arrows indicate the positions of the in-plane inter-DNA correlation peaks. Note the large change in the DNA peak positions in the negatively overcharged complexes (b), due to the condensation of DNA into close-packed 2-D rafts. Note also the absence of the DNA condensation transition for the positively overcharged complex (a). This condensation behavior is the similar to that observed for complexes with monodisperse λ-DNA.

(30/70 DOTAP/DOPC membrane charge density) without added Cd^{2+} (see curve 1 in Figure 3b), the peaks correspond to a lamellar periodicity of 70.0 Å. Those lamellar periodicities are slightly larger than those of the corresponding isoelectric complexes. It is interesting to note that no DNA condensation is observed for positively overcharged complexes ($D/L < 1$). In contrast, for the negatively overcharged complexes ($D/L > 1$), DNA exhibits behavior analogous to that of isoelectric complexes and condenses at sufficiently high global [Cd^{2+}]. These trends can be seen in the two typical sets of SAXS data in Figure 3 for overcharged λ-phage DNA−membrane complexes. For positively overcharged complexes ($D/L = 0.6$, 70/30 DOTAP/DOPC membrane, Figure 3a), the initial d_{DNA} is 37.8 Å (compare with 29.8 Å for the corresponding isoelectric complex of the same membrane charge density, curve 1 in Figure 2a). As [Cd^{2+}] is increased, d_{DNA} remained unchanged. For negatively overcharged complexes ($D/L = 1.4$, 30/70 DOTAP/DOPC membrane, Figure 3b), the initial d_{DNA} is 45.8 Å (compare with 58.1 Å for isoelectric complex of the same membrane charge density, curve 1 in Figure 2b). As [Cd^{2+}] is increased, the inter-DNA spacing decreases in the same manner as the isoelectric complexes and reaches a 2D condensed DNA state.

3.3. Effects from DNA Polydispersity. We have investigated the effects of DNA polydispersity on the biomolecular templating process using DNA-membrane complexes. λ-phage DNA is monodisperse, with a contour length of $\sim$16.5 μm. We have compared the templating behavior of λ-DNA with that of highly polydisperse calf thymus DNA, which has a contour length ranging from 10^{-2} to 10^{2} μm. Calf thymus DNA is significantly less expensive than λ-DNA and is potentially better suited for templating large quantities of nanocrystals. A set of typical SAXS data for isoelectric calf thymus DNA−membrane complexes at different global [Cd^{2+}] are shown in Figure 4. The lamellar phase is preserved, and the characteristic diffraction signature of a regularly spaced series of diffraction peaks can clearly be observed. These peaks correspond to a lamellar periodicity of 62.2 and 68.1 Å for the 70/30 and 30/70 membrane, respectively, which agrees well with the lamellar periodicity for isoelectric λ-phage DNA−membrane complexes. The general behavior of the isoelectric calf thymus DNA-based complexes is basically the same as that for the λ-DNA based complexes, although the inter-DNA separation d_{DNA} is slightly different under the same conditions. For example, the initial d_{DNA} of the complexes made by 70/30 DOTAP/DOPC lipids and calf thymus DNA is 32.5 Å. The corresponding correlation peak partially overlaps with the low q side of the 2nd order lamellar correlation peak (see curve 1 in Figure 4 a). In contrast, the initial d_{DNA} of the complexes made by 70/30 DOTAP/DOPC lipids and λ-phage DNA is 29.8 Å, and the corresponding correlation peak partially overlaps with the high q side of the 2nd order lamellar correlation peak (see curve 1 in Figure 2a). The same generic DNA condensation behavior at high [Cd^{2+}] is observed for isoelectric calf thymus DNA−membrane complexes at all membrane charge densities studied. The behavior for nonisoelectric complexes is also similar. Typical SAXS data for overcharged calf thymus DNA−membrane complexes at different global [Cd^{2+}] are shown in Figure 5. Elevating global [Cd^{2+}] has no impact on the positively overcharged complexes, and no DNA condensation is observed. For negatively overcharged complexes, DNA condensed at a threshold concentration of Cd^{2+} in the same way as the isoelectric complexes.

In summary, the behavior of DNA−membrane complexes in the presence of Cd^{2+} with either λ-phage DNA or calf thymus DNA is similar. In both cases, the interhelical DNA spacing can be precisely controlled by a combination of global [Cd^{2+}] and DNA−lipid charge stoichiometry, although the absolute

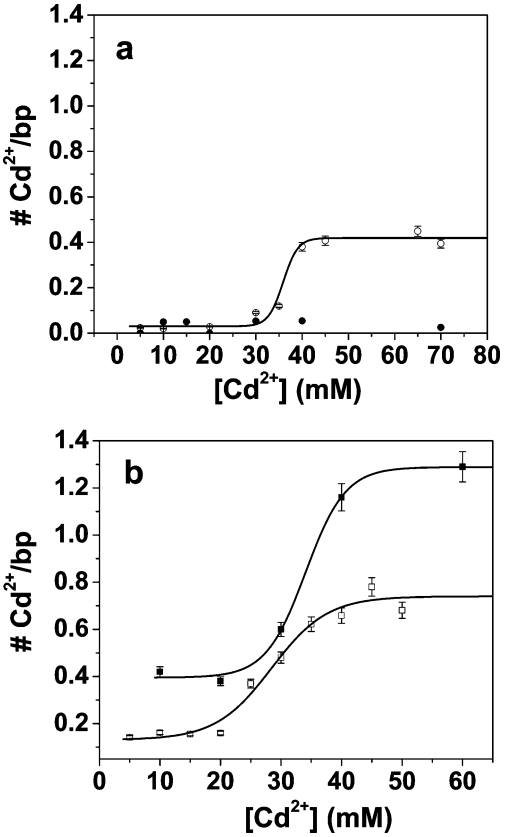

Figure 6. Condensed Cd^{2+} ion density inside DNA−membrane template systems at different global $[Cd^{2+}]$ measured by ICPOES. (a) 70/30 DOTAP/DOPC membrane (○, isoelectric; ●, $(-)_{DNA}/(+)_{membrane} = 0.6$); (b) 30/70 DOTAP/DOPC membrane (□, isoelectric; ■, $(-)_{DNA}/(+)_{membrane} = 1.4$). For isoelectric and negatively overcharged DNA−membrane complexes, Cd^{2+} can drive DNA condensation. As the DNA strands condense (as measured by X-ray diffraction), additional Cd^{2+} ions are recruited and organized between the DNA strands in the close-packed DNA rafts. For positively overcharged complexes, DNA condensation does not occur, and no additional Cd^{2+} ions are condensed into the complexes. Local concentration of condensed Cd^{2+} in the nanopores can be as high as ∼2.50 M, even though the global Cd^{2+} concentration is only ∼10's of mM.

values of the DNA spacing are different for the two cases. This can be best seen by comparing the DNA correlation peak under the arrows for the two different kinds of DNA at the same conditions (Figures 2, 3 versus Figures 4, 5). The inter-DNA spacing within the DNA−membrane complex essentially defines the nanopore sizes in which the CdS nanocrystals are templated.

3.4. Density of Cd^{2+} Ions within DNA−Membrane Complexes. Besides nanopore size, another important parameter for the DNA−membrane templating process is the precursor ion (Cd^{2+}) density inside the DNA−membrane complexes, which defines the average initial interion spacing before CdS crystal growth. Since DNA−membrane complexes precipitate out of solution and can be separated by centrifugation, the Cd^{2+} ion density sequestered inside the complexes can be estimated by measuring $[Cd^{2+}]$ in the supernatant. This can be subtracted from the known global $[Cd^{2+}]$ to get the number of Cd^{2+} ions condensed in the DNA−membrane complexes. Inductively coupled plasma optical emission spectroscopy (ICPOES) is used to measure $[Cd^{2+}]$ in all the samples. The ICPOES data for calf thymus DNA−membrane complexes at different membrane charge densities, different DNA-to-lipid charge stoichiometries, and different global $[Cd^{2+}]$ are shown in Figure 6. For isoelectric and negatively overcharged DNA−membrane complexes, an

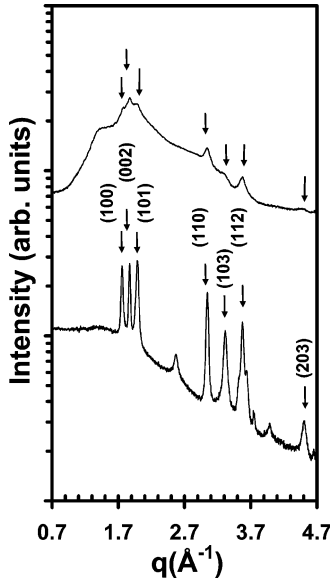

Figure 7. WAXS of templated CdS compared with CdS grown in free solution. Top curve: a typical DNA−membrane complex (isoelectric calf thymus DNA self-assembled with 30/70 DOTAP/DOPC membrane at global $[Cd^{2+}] = 40$ mM) after H_2S reaction. Bottom curve: CdS grown in 40 mM $[CdCl_2]$ solution under the same conditions without the biomolecular templates. The arrows indicate the characteristic diffraction peaks from the CdS wurtzite structure in both cases. Note the peaks from templated CdS are significantly wider, due to their nanoscopic size.

increase in the number of condensed Cd^{2+} ions is observed at $[Cd^{2+}]$ near the threshold concentration where 2D DNA condensation is observed in X-ray diffraction (see ○ in Figure 6a; □, ■ in Figure 6b). This suggests that as DNA condensation occurs, additional Cd^{2+} ions are condensed and organized between the DNA strands in the close-packed DNA rafts. In contrast, increasing the global $[Cd^{2+}]$ has no effect on the structure of positively overcharged DNA−membrane complexes, and no additional Cd^{2+} ions are condensed into the complexes (see ● in Figure 6a). The ICPOES data are a quantitative measure of Cd^{2+} ion condensation within the complexes: for complexes with DOTAP/DOPC = 70/30, the maximum condensed Cd^{2+} ions density (e.g., Cd^{2+} ions density inside the complexes after DNA condensation) is ∼0.4 Cd^{2+} ion per base pair of DNA (Cd^{2+}/bp), while, for DOTAP/DOPC = 30/70, the maximum condensed ion density is ∼0.7 Cd^{2+}/bp (see ○ in Figure 6a, and □ in Figure 6b).

The behavior of the lamellar spacing between the membrane sheets during the DNA condensation is interesting in the context of these condensed ion density measurements. Recall that the observed expansion of the lamellar spacing after DNA condensation is 2.6 Å for the high membrane charge density DOTAP/DOPC = 70/30 complexes and 4.9 Å for the low membrane charge density DOTAP/DOPC = 30/70 complexes. This is consistent with the observation that there are fewer condensed Cd^{2+} ions in the high membrane charge density sample than the low membrane charge density sample, as indicated by the ICPOES measurements. For complexes with the same membrane charge density but different DNA-to-lipid charge stoichiometries, the number of condensed Cd^{2+} ions is changed. Negatively overcharged complexes are able to condense more Cd^{2+} ion precursors than isoelectric complexes. For example, for complexes with DOTAP/DOPC = 30/70, the condensed Cd^{2+} density is ∼1.2 Cd^{2+}/bp when $D/L = 1.4$ but decreases to

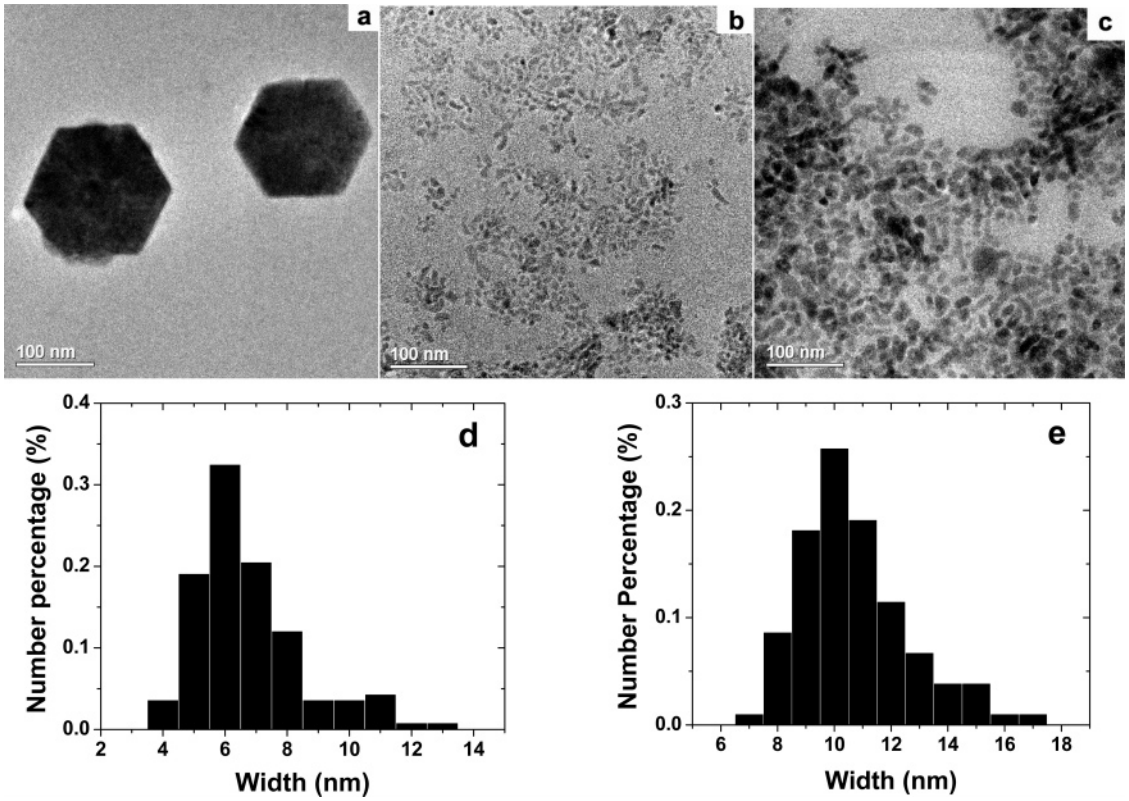

Figure 8. Low resolution TEM images of CdS grown in free solution compared with that templated by DNA−membrane complexes. CdS is grown by reacting H_2S with (a) 40 mM $CdCl_2$; (b) isoelectric calf thymus DNA−70/30 DOTAP/DOPC membrane complexes at global $[Cd^{2+}] = 40$ mM; (c) isoelectric calf thymus DNA−30/70 DOTAP/DOPC membrane complexes at global $[Cd^{2+}] = 40$mM. Images d, e show the statistical distribution of templated CdS nanorod widths in images b and c, respectively. The widths of templated CdS nanorods are controlled by the initial condensed Cd^{2+} ion densities, which are in turn controlled by membrane charge density and/or DNA-to-lipid charge stoichiometry.

$\sim$0.7 Cd^{2+}/bp when $D/L = 1$ (see Figure 6 b), suggesting that as more charged lipids are incorporated into the DNA−membrane complex, the number of condensed Cd^{2+} ions will decrease in the complex. By comparison, positively overcharged complexes do not exhibit DNA condensation with increasing Cd^{2+} ion density (see ● in Figure 6a), indicating that the membrane surface charge density is a crucial control parameter in the templating process.

Since the structure and dimensions of self-assembled DNA−membrane complexes are known for different global $[Cd^{2+}]$, we can calculate $[Cd^{2+}]$ inside the nanopores of the template systems. For example, for isoelectric complexes comprised of calf thymus DNA with 70/30 DOTAP/DOPC membrane composition at global $[Cd^{2+}] = 10$ mM, the measured Cd^{2+} density inside complexes is $\sim$0.02 Cd^{2+}/bp. The interhelical DNA spacing is $\sim$34 Å from the X-ray measurements above. The hydrated DNA diameter is known to be $\sim$25 Å, and the base pair spacing is $\sim$3.4 Å. The condensed Cd^{2+} density is equivalent to a $[Cd^{2+}]$ of 0.02/1222 Å^3, or $\sim$27 mM, which is close to the global $[Cd^{2+}]$. However, after DNA condensation at global $[Cd^{2+}] = 40$ mM, the condensed Cd^{2+} ion density inside complexes was measured as $\sim$0.4 Cd^{2+}/bp. Given that the measured interhelical DNA spacing is $\sim$27 Å, this condensed Cd^{2+} concentration is $\sim$0.4/627 Å^3, or $\sim$1.06 M, which is much higher than the 40 mM global $[Cd^{2+}]$. Complexes with lower membrane charge densities are able to condense more Cd^{2+} ions. For isoelectric complexes made up by calf thymus DNA with 30/70 DOTAP/DOPC membrane, the condensed Cd^{2+} ions density (at global $[Cd^{2+}] = 40$ mM) is measured to be $\sim$0.7 Cd^{2+}/bp. The interhelical DNA spacing is $\sim$29 Å from X-ray diffraction; therefore the ion density is approximately $[Cd^{2+}] \approx 0.7/797$ Å^3, or $\sim$1.46 M in the nanopores. Even higher condensed Cd^{2+} ions densities can be obtained for negatively overcharged complexes. For negatively overcharged complexes ($D/L = 1.4$) comprised of calf thymus DNA and DOTAP/DOPC = 30/70 membranes, the condensed Cd^{2+} ions density is $\sim$1.2 Cd^{2+}/bp. A similar estimate gives an average ion concentration of $[Cd^{2+}] \approx 2.50$ M in the DNA nanopores. The local Cd^{2+} concentrations are likely to be even higher, since higher condensed Cd^{2+} ion concentrations are expected near the negatively charged DNA sugar−phosphate backbone. From these estimates, it can be seen that typical condensed Cd^{2+} ions densities in the DNA−membrane template systems is approximately one-tenth that of the Cd concentration in bulk CdS crystals, which is $\sim$1/100 Å^3, or $\sim$17 M. The Cd concentration in CdS crystals is significantly higher than that within the templates and suggests that diffusional transport of both anions and cations within the complex during growth is important for the templating process.

3.5. Structural Characterization of the CdS Grown within DNA−Membrane Templates. Using a combination of membrane charge density, DNA-to-lipid charge ratio, and global $[Cd^{2+}]$, structural parameters of the DNA−membrane template such as the condensed ion density and the nanopore size can be controlled. DNA-membrane complexes with condensed Cd^{2+} ions are reacted with H_2S in the gas phase to form CdS nanocrystals at room temperature. The existence of CdS is confirmed using Wide-angle X-ray scattering (WAXS). CdS

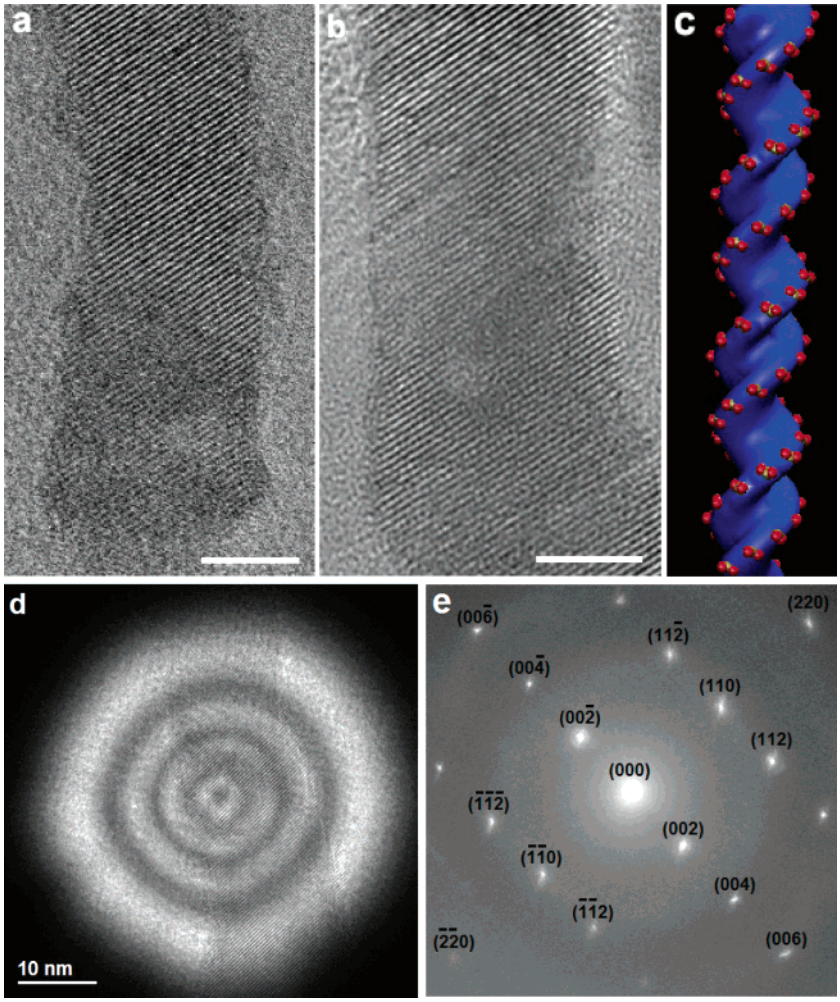

Figure 9. Molecular casting of CdS nanorods. (a, b) HRTEM images of typical individual CdS nanorods templated by isoelectric DNA−membrane complexes comprised of 30/70 DOTAP/DOPC membrane with λ-phage DNA (a) or calf thymus DNA (b) (scale bar is 5 nm). Note 60° tilt of (002) planes relative to rod axis. (c) Schematic representation of B-form DNA, showing the negatively charged phosphate groups (red) on the backbone, which organize the Cd^{2+} ions and guide the nucleation of CdS; (d) Single nanorod diffraction reveals the crystallographic structure of the templated CdS nanorods. A single CdS nanorod (different from that shown in parts a and b) is illuminated by an electron beam probe, with a probe size of ~43 nm. Note the tilt of (002) lattice fringes. (e) Resultant nanobeam diffraction pattern of the CdS nanorod in part d. The zone axis is [1$\bar{1}$0]. The single rod diffraction pattern unambiguously indicates the tilt of the (002) planes.

nanocrystals confined in DNA−membrane complexes have been studied with WAXS and compared with CdS grown in free solution at the same conditions. A typical result is shown in Figure 7. The CdS grown in free solution have a wurtzite structure (bottom curve), and the seven strongest peaks belonging to the wurtzite structure factor can be seen. The corresponding peaks (denoted with arrows) are also visible in the WAXS data for CdS nanocrystals confined in DNA−membrane complexes (see top curve), indicating that the CdS grown in the nanopores of the biomolecular template system also has the wurtzite structure. Note the peaks from templated CdS are significantly wider, which is expected for crystals of nanoscopic size.

CdS grown in DNA−membrane complexes can be isolated by dissolving away the organic template matrix in ~1% sodium dodecyl sulfate solution. The CdS crystals grown in complexes with different initial condensed Cd^{2+} ion densities have been studied by transmission electron microscope (TEM) and compared with the CdS grown in free solution. The morphology of templated CdS is completely different from that of CdS grown in free solution (see Figure 8). CdS grown in free solution are micron-sized single crystals with a hexagonal shape. However, CdS grown in DNA−membrane complexes are one-dimensional rodlike nanocrystals. No changes of width are observed by tilting these nanocrystals under the TEM, suggesting that the rodlike shape is quite symmetrical. The condensed Cd^{2+} ions are confined in arrays of nanopores in DNA−membrane complexes, which are aligned along the DNA axis. This implies that, during the H_2S reaction, the CdS growth is confined in directions perpendicular to the DNA axis and is unconfined along the DNA, hence resulting in rodlike nanocrystals.

The widths of templated CdS nanorods are different for different initial condensed Cd^{2+} ion densities. The statistics for the widths of templated CdS rods are shown in Figure 8d and e. For isoelectric DNA−70/30 DOTAP/DOPC membrane complexes (condensed Cd^{2+} ions density ~0.4 Cd^{2+}/bp), the average nanorod width is ~6 ± 1 nm; whereas, for isoelectric DNA-30/70 DOTAP/DOPC membrane complexes (condensed Cd^{2+} ions density ~0.7 Cd^{2+}/bp), the average nanorod width is ~10 ± 1 nm. Clearly, the widths of templated CdS nanorods can be effectively controlled by the initial condensed Cd^{2+} ion densities, which in turn can be controlled by membrane charge

density and/or DNA-to-lipid charge stoichiometry. It must be emphasized that it is the concentration of condensed ions rather than the nanopore size that controls the templated CdS nanorod width. Moreover, it is interesting to note that it is the width rather than the length that is controlled. The aspect ratios for the nanorods are inhomogeneous and range from ~1 to ~10.

Anionic and cationic components in the DNA−membrane template work synergistically together in the templating process: DNA is highly anionic. The mean distance between negative charges on DNA (0.17 nm) is less than the Bjerrum length (0.78 nm), defined as $e^2/\epsilon kT$, where e is an elementary charge, ϵ is the static dielectric constant, k is the Boltzmann constant, and T is the temperature. This implies that the linear charge density of DNA is beyond the Manning limit, and a layer of condensed ions, in the present case Cd^{2+}, is expected to condense on its surface.[53−55] The concentration of Cd^{2+} ions condensed on the DNA within the composite DNA−membrane template, which determines the final CdS morphology, is modulated by the charge density of the cationic membrane. A similar interplay between anionic and cationic components in biomolecular templates may be operative in more complex biomineralization systems.

Current approaches for making wurtzite II−VI semiconductor nanorods exploit the anisotropic growth rates for different lattice planes. For this reason, the growth direction is usually along the *c*-axis; e.g., the (002) planes are usually perpendicular to the rod direction.[56−58] Surprisingly, nanorods grown from the DNA−membrane complexes are not oriented along the *c*-axis. This is clearly seen in the two different high-resolution TEM (HRTEM) images of representative nanorods (Figure 9a,b), templated from isoelectric complexes of calf thymus DNA with 30/70 DOTAP/DOPC membrane with global $[Cd^{2+}]$ at 40 mM. The lattice fringes correspond to (002) planes of CdS ($d = 0.336$ nm), which are tilted by 60° from the rod axis, in contrast to all known wurtzite nanorods prepared from other approaches. This observed tilt of the (002) lattice planes can be related to the orientation of the DNA sugar−phosphate backbone, which is tilted by ~60° with respect to the helix axis in B-form DNA when projected onto a 2D plane (Figure 9c).[59] The spatial distribution of the positively charged Cd^{2+} ions, and therefore the nucleation of the CdS polar (002) planes, is organized by this negatively charged "ridge" on the DNA surface. In fact, recent experiments have shown that it is possible for biopolymers to spatially organize ions on the nanometer scale via electrostatic interactions.[60] Because the templated CdS nanorods are confined to grow along the nanopores defined by adjacent DNA strands, the (002) planes are tilted by ~60° with respect to the nanorod major axis. The periodicity of each helical turn of B-form DNA is ~3.4 nm, which is just enough to fit 10 (002) planes with nearly no mismatch. This unusual crystallographic orientation was further confirmed by nanobeam diffraction (NBD). In these NBD measurements, a 43 nm diameter electron beam probe is used to illuminate a single nanorod with (002) planes tilted ~60° away from the rod direction (see Figure 9d). The diameter of the probe beam can be seen relative to the width of the horizontally oriented CdS nanorod, on which lattice fringes can be clearly observed. The resultant diffraction pattern of the single nanorod is shown in Figure 9e and confirms the crystallographic orientation of the (002) planes with respect to the long axis of the nanorod.

4. Conclusions

In summary, we have investigated how the anionic and cationic components of DNA−membrane templates affect the CdS templating process. Depending on the charge of the membrane, different concentrations of Cd^{2+} ions are condensed into the template, and different morphologies of CdS are templated as a result. The condensed Cd^{2+} ion concentration can also be independently controlled by the degree of template overcharging, as determined by the relative stoichiometry of DNA and cationic membrane lipids. For example, no significant amount of Cd^{2+} is condensed into the template for positively overcharged templates, while negatively overcharged templates condense more Cd^{2+} ions than isoelectric templates. The condensed Cd^{2+} ion concentrations inside the DNA nanopores can be as high as 2.5 M, which is almost 100× greater than that of the ambient concentrations. The DNA−membrane templating system tolerates DNA polydispersity quite well, since CdS can be grown using polydisperse calf thymus DNA. This implies that it is not necessary to use monodisperse polyelectrolytes. Finally, crystallographic control of the inorganic nanostructures is possible using DNA−cationic membrane complexes. The strong electrostatic interactions within such complexes align the CdS (002) polar planes parallel to the negatively charged sugar−phosphate DNA backbone, which suggests that molecular details of the DNA molecule have been replicated onto the inorganic crystal structure.

Acknowledgment. This work is based in part upon work supported by the U.S. Department of Energy, Division of Materials Sciences, under Award No. DEFG02-91ER9645439, through the Frederick Seitz Materials Research Laboratory at the University of Illinois at Urbana-Champaign, and by the National Science Foundation NSEC DMR-0117792. Research for this publication was carried out in the Center for Microanalysis of Materials, University of Illinois at Urbana-Champaign, which is partially supported by the U.S. Department of Energy under grant DEFG02-91-ER45439. We are also grateful to Jianguo Wen and Jianmin Zuo for helpful discussions.

JA046718M

(53) Levin, Y. *Rep. Prog. Phys.* **2002**, *65*, 1577−1632.
(54) Manning, G. S. *Q. Rev. Biophys.* **1978**, *16*, 179−246.
(55) Holm, C., Kekicheff, P., Podgornik, R., Eds. *Electrostatic Effects in Soft Matter and Biophysics*; Kluwer Academic Publishers: 2001.
(56) Peng, X. G.; Manna, L.; Yang, W. D.; Wickham, J.; Scher, E.; Kadavanich, A.; Alivisatos, A. P. *Nature* **2000**, *404*, 59−61.
(57) Duan, X. F.; Lieber, C. M. *Adv. Mater.* **2000**, *12*, 298−302.
(58) Manna, L.; Scher, E. C.; Alivisatos, A. P. *J. Am. Chem. Soc.* **2000**, *122*, 12700−12706.
(59) Sinden, R. R. *DNA Structure and Function*; Academic Press: New York, 1994.
(60) Angelini, T. E.; Liang, H.; Wriggers, W.; Wong, G. C. L. *Proc. Natl. Acad. Sci. U.S.A.* **2003**, *100*, 8634−8637.